

# Time-dependent simulations of emission from FSRQ PKS 1510–089: multiwavelength variability of external Compton and SSC models

Xuhui Chen,<sup>1\*</sup> Giovanni Fossati,<sup>1\*</sup> Markus Böttcher<sup>2</sup>, and Edison Liang<sup>1</sup>

<sup>1</sup> Department of Physics and Astronomy, Rice University, Houston, TX 77005

<sup>2</sup> Astrophysical Institute, Department of Physics and Astronomy, Ohio University, Athens, OH 45701

Accepted 2012 May 9. Received 2012 May 8; in original form 2012 March 31

## ABSTRACT

We present results of modeling the broadband SED and multiwavelength variability of the bright FSRQ PKS 1510–089 with our time-dependent multizone Monte Carlo/Fokker-Planck code (Chen et al. 2011b). As the primary source of seed photons for inverse Compton scattering, we consider radiation from the broad line region (BLR), from the hot dust of the molecular torus, and the local synchrotron radiation (synchrotron-self-Compton, SSC). We evaluate the viability of different Compton models by comparing simulated multiwavelength light curves and SEDs with one of the best observed flares by PKS 1510–089, in March 2009. The time-dependence of our code and its correct handling of light travel time effects allow us to fully take into account the effect of the finite size of the active region, and in turn to fully exploit the information carried by time resolved observed SEDs that are becoming increasingly available since the launch of *Fermi*. We confirm that the spectrum adopted for the external radiation field has an important impact on the modeling of the SED, in particular for the lower energy end of the Compton component which is observed in the X-ray band, which in turn is one of the most critical bands to assess the differences between EC and SSC emission. In the context of the scenario presented in this paper, where the flaring is caused by the increase of the number of relativistic electrons ascribed to the effect of the interaction of a portion of the jet (blob) with a shock, we can not firmly discriminate the three main scenarios for  $\gamma$ -ray emission. However, results show clearly the differences produced by a more realistic treatment of the emitting source in the shape of SEDs and their time variability over relevant, observable time-scales, and demonstrate the crucial importance of time-dependent multi-zone models to advance our understanding of the physics of these sources, by taking full advantage of the wealth of information offered by the high quality data of current multiwavelength campaigns.

**Key words:** galaxies: active – galaxies: jets – X-rays: theory

## 1 INTRODUCTION

The spectral energy distributions (SED) of blazars usually show two major non-thermal components. The low energy one, peaking in the IR – optical – X-ray range is identified as synchrotron radiation. The origin of the high energy one, peaking in the  $\gamma$ -ray energy range (MeV to TeV) is less clear. Proposed ideas include leptonic models, based on inverse Compton (IC) scattering by the same electrons emitting the synchrotron radiation, and hadronic models, in which protons play a critical role in producing the high energy emission (Mannheim 1998; Rachen 2000; Sikora & Madejski 2001; Arbeiter et al. 2005; Levinson 2006; Böttcher 2007; Dermer & Lott 2011). For the leptonic IC-based models, several sources of the target photons are possible and the

debate about which one is dominant and in which type of object has recently been reignited. If the seed photons are provided by the synchrotron radiation emitted at lower energy by the same IC-scattering electrons, it is referred to as synchrotron self-Compton (SSC). Scenarios in which the dominant contribution to the seed soft photon field for IC is provided by radiation emitted elsewhere are referred to as external Compton (EC) models. External sources of seed photons may include the photons from accretion disc, hot X-ray-emitting corona, broad emission line region, infrared torus, host galaxy bulge, and cosmic background radiation (Ghisellini & Tavecchio 2009).

There are two major classes of blazars: BL Lac objects, which have featureless optical spectra, and Flat Spectrum Radio Quasars (FSRQ), which exhibit broad quasar-like emission lines. The presence of these latter in FSRQs suggests that their jets are in an environment with a stronger external radiation field. Furthermore, de-

\* gfoassati@rice.edu, xuhui.chen@alumni.rice.edu

pending on the relative location of these sources external to the jet and of active jet region (blob), the emission from the external sources would be relativistically beamed and enhanced in the frame of the blob, possibly making them dominant over the locally produced synchrotron emission. Therefore, the EC model is frequently invoked to explain the emission of FSRQs (Dermer et al. 1992; Sikora et al. 1994, 2009).

A major defining feature of blazars is their rapid and large variability, observed over the entire range of their continuum emission (radio to TeV  $\gamma$ -rays). Simultaneous multiwavelength observations and the correlation analysis of the observed multiwavelength variability can provide insights to the physics of particle processes and radiation mechanisms in the jet. The detailed observation and modeling of such variability has been performed extensively for High energy peaked BL Lacs (HBL) such as Mrk 421 (Fossati et al. 2008; Chen et al. 2011b) and PKS 2155–304 (Aharonian et al. 2007; Katarzyński et al. 2008). In the case of HBLs, such studies are facilitated by their synchrotron SED peak falling in the X-ray range which can be observed with multiple X-ray satellites, while their high energy SED peak in TeV  $\gamma$ -ray is covered by ground based Atmospheric Cherenkov Telescopes (for a review, Hinton & Hofmann 2009; examples for Mrk 421, Fossati et al. 2008; Abramowski et al. 2012).

The launch of *Fermi* has re-opened the GeV  $\gamma$ -ray sky with unprecedented sensitivity and daily coverage. This energy band covers a highly variable part of the SED right above the peak of the high energy component of the SED of several bright FSRQs, such as PKS 1510–089 (Abdo et al. 2010a) and 3C454.3 (Abdo et al. 2009). Simultaneous coverage in other wavelength such as optical and X-rays provided us a chance to obtain multi-epoch SEDs and cross-band correlations. A deeper understanding of these time series data sets requires time-dependent modeling with all light travel time effects (LTTEs) taken into account.

The importance of the LTTE in the study of blazars has long been realized (Chiaberge & Ghisellini 1999). The observed change of flux level on time-scale of hours in some blazars indicates that these effects must have a large impact on the variability of blazars. There have been some efforts to include these effects in the modeling of blazars (Kataoka et al. 2000; Sokolov et al. 2004; Sokolov & Marscher 2005; Katarzyński et al. 2008; Graff et al. 2008), but none of them have taken into account all of these effects in a generic 2D geometry.

We have developed a time-dependent multizone code using the Monte Carlo method for radiation transport and the Fokker-Planck equation for electron evolution, which we first applied to a study of the correlated X-ray/ $\gamma$ -ray variability of the HBL Mrk 421 using a pure SSC model (Chen et al. 2011b). In this paper we extend the model to include external sources of IC seed photons and apply it to study the multiwavelength variability of an archetypical powerful FSRQ, PKS 1510–089.

## 2 PKS 1510–089

PKS 1510–089 is a FSRQ at a redshift of  $z = 0.361$  (Thompson et al. 1990). It is one of the brightest and most variable sources detected by *Fermi*/LAT. A feature that can be interpreted as disk emission (big blue bump, BBB) is clearly visible in its optical/UV spectrum. VLBI observations of its jet show superluminal motion with apparent speed up to  $45c$  ( $\Gamma = 36$ , Jorstad et al. 2005).

Since the advent of *Fermi*, the long-term multiwavelength

monitoring effort, complemented by more intense campaigns motivated by flaring phases, has led to the observation of several large correlated flares for PKS 1510–089 (Abdo et al. 2010b,a; D’Ammando et al. 2011; Marscher et al. 2010; Kataoka et al. 2008; Pucella et al. 2008).

As reference data for our simulation we choose the observations of a high state observed in 2008–2009 and presented by Abdo et al. (2010a), D’Ammando et al. (2011) and Marscher et al. (2010). One particular flare at the end of March 2009 (peaking around March 25th, MJD 54917) is chosen as the benchmark for this study.

We aim to reproduce several observational features by matching both the simulated light curves and SED with the observed ones. These features include:

- Clear presence of BBB emission with the general two non-thermal continuum components SED. The BBB is evident in both the high and the low states of the jet non-thermal continuum emission.
- The time-scale of the flares, which were typically about 4 days (300 ks) at all wavelengths.
- Infrared and  $\gamma$ -ray light curves show the stronger variations among the observed bands, with similar amplitude, up to a factor of 10. In the March 2009 flare, the infrared (R band) and  $\gamma$ -ray (*Fermi*/LAT) fluxes were strongly correlated, with no significant lags.
- The variations in the *Swift*/UVOT bands were less prominent than those in the infrared – optical bands. The optical/UV spectral shape became softer when the source brightness increased, consistent with the combination of a variable softer broad band continuum (synchrotron) and a non variable component peaked in the UV band (BBB).
- The variability in the X-ray band luminosity was modest, within a factor of 2 over a period of 4 months encompassing the flare that we selected for this study (*Swift*/XRT in Abdo et al. 2010a, *RossiXTE*/PCA in Marscher et al. 2010). The spectrum was always very hard, with energy index  $\alpha_X < 0.6$  ( $F_\nu \propto \nu^{-\alpha}$ ) with very little variability. During the period around the benchmark flare it remained  $\alpha_X \simeq 0.5$  (Abdo et al. 2010a).
- The  $> 0.2$  GeV spectral shape as measured by *Fermi*/LAT did not vary significantly through large luminosity changes, remaining around  $\alpha_\gamma \simeq 1.5$  (for a power law fit) (Abdo et al. 2010a).

These characteristics only coarsely summarize the true richness of information provided by the full multiwavelength and multi-epoch data set which thanks to our simulations we can try to exploit more deeply. Nevertheless, because they constitute a quicker and easier way of guiding the setup and evaluation of the simulations and we will refer to them when discussing the comparison of our simulation results with observations in the following sections.

## 3 SIMULATIONS

### 3.1 Basic setup and model parameters

Details and technical aspects of our Monte Carlo/Fokker-Planck code are described in Chen et al. (2011b, Chen 2012, Chen et al. in preparation). The code uses the Monte Carlo method to track the production, travel, and Compton scattering of photons, while it solves the isotropic Fokker-Planck equation to follow the evolution of electrons. The major strength and unique feature of this code is that it takes into account all the LTTEs, internal to the source volume (e.g. important for IC emission) and external, i.e. their effect

**Table 1.** Summary of model parameters

Parameter	nf/blr	blr15	blr15highgmin	blr25	torus15	ssc
Jet bulk Lorentz factor, $\Gamma$	15.0	15.0	15.0	25.0	15.0	10.0
$Z$ ( $10^{16}$ cm)	8.0	8.0	8.0	13.33	8.0	5.0
$R$ ( $10^{16}$ cm)	6.0	6.0	6.0	10.0	6.0	3.75
Magnetic field, $B$	0.3	0.3	0.3	0.16	0.2	0.1
Particle density (initial), $n_e$ ( $10^4$ cm $^{-3}$ )	2.66	2.66	2.66	0.14	$7.37 \cdot 10^{-2}$	0.01
Particle escape time-scale, $t'_{\text{esc}}$ ( $Z/c$ )	0.1	0.1	0.1	0.1	0.015	0.03
Particle (diffuse) acceleration time-scale, $t'_{\text{acc}}$ ( $Z/c$ )	0.55	0.55	0.55	0.55	0.09	0.19
Electron pick up rate, $Q_{\text{pick}}$ (cm $^{-3}$ s $^{-1}$ )	0.1	0.1	0.1	$3.2 \cdot 10^{-3}$	0.0191	0.002
Pick-up electrons energy, $\gamma_{\text{pick}}$	5.0	5.0	5.0	5.0	50.0	1200.0
Shock injection: $\gamma_{\text{min},\text{inj}}$	...	30	90	6	300	2000
Shock injection: $\gamma_{\text{max},\text{inj}}$	...	$2 \cdot 10^4$	$2 \cdot 10^4$	$4 \cdot 10^3$	$2 \cdot 10^5$	$10^5$
Shock injection: power-law slope, $p_{\text{inj}}$	...	3.2	3.2	3.2	3.2	3.2
Shock injection: rate: $L'_{\text{inj}}$ ( $10^{44}$ erg s $^{-1}$ )	...	3.5	2.0	2.8	5.0	8.0
$R_{\text{BLR}}$ or $R_{\text{IR}}$ ( $10^{18}$ cm)	0.8	0.8	0.8	0.8	7.8	...
$f_{\text{BLR}}$ or $f_{\text{IR}}$	0.013	0.013	0.013	0.0015	0.5	...

on the observed radiation which we will receive at different times depending on where it was emitted in the source.

We model a jet active region (blob) as a cylindrical volume crossing a standing ‘shock’ as illustrated in Fig.1. In the blob rest frame, where all calculations are performed, the shock moves through the cylindrical region with a speed equal to the bulk velocity of the blob  $v_{\text{bulk}} \sim c$ . The cylindrical volume is divided evenly into zones in the radial and vertical directions ( $r$  and  $z$  coordinates,  $n_r, n_z$ ). In all runs presented in this paper,  $n_r = 9$  and  $n_z = 30$ .

At this stage the meaning of this shock is simply that of an agent affecting the properties of the simulation zone where it is at a given time. In the simulations presented in this paper it affects the electron distribution, namely it injects high energy particles into the zones it currently resides in. It does not affect the magnetic field, which is assumed to be homogeneous throughout the volume and

non varying. The shock has not thickness (however, our resolution is limited by  $dz$ ) and is treated as a surface perpendicular to the  $z$  direction.

With respect to the simulations presented in (Chen et al. 2011b), we added a few features to the code. The most relevant ones are the inclusion of a spatially diffuse stochastic acceleration process, similar to the one discussed by Katarzyński et al. (2006), of a particle escape term and of a particle ‘pick-up’ term (see also Tramacere et al. 2011). These developments and their motivation are discussed in Chen et al. (2011a), Chen (2012) and Chen et al. (2012). We treat stochastic acceleration in the whole blob as a diffusive term in the Fokker-Planck equation, while the putative first order Fermi acceleration at the shock front is simplified as directly injecting high energy particles with a power law distribution into the zones where the shock is present.

The main parameters of the model are (see also Table 1):

- $\Gamma$ , the bulk Lorentz factor of the jet.
- $R$  and  $Z$ , the radius and height of the cylindrical simulation region.
- $B$ , the magnetic field strength, assumed here to be homogeneous and non variable.
- $n_e$ , the initial electron number density.
- $t'_{\text{acc}}$  and  $t'_{\text{esc}}$ , the time-scales parameterizing the stochastic diffuse acceleration and particle escape.
- $Q_{\text{pick}}$ , the rate at which the blob constantly picks up mildly relativistic electrons (with a narrow Gaussian distribution centered at  $\gamma_{\text{pick}}$ ).
- $L'_{\text{inj}}$ , the luminosity of the relativistic electrons injected by the shock.
- $p_{\text{inj}}$ ,  $\gamma_{\text{min},\text{inj}}$  and  $\gamma_{\text{max},\text{inj}}$  are the spectral index, minimum and maximum Lorentz factor of the electrons injected locally by the shock with a power law spectrum.
- $R_{\text{BLR}}$ ,  $f_{\text{BLR}}$  are the size of the broad line region, assumed to be spherical and the fraction of the luminosity from the accretion disk that contributes to the radiation energy density within its volume.  $R_{\text{IR}}$  and  $f_{\text{IR}}$  are the corresponding parameters for the case of the infrared emitting torus. Collectively we also call them  $R_{\text{ext}}$  and  $f_{\text{ext}}$  without distinction between BLR and IR. We will discuss them in the following sections.

At the beginning of a simulation each zone of the blob is filled with electrons with density  $n_e$  and a power law spectrum with slope and energy range given by  $p$ ,  $\gamma_{\text{min}}$  and  $\gamma_{\text{max}}$ . The same parameters are used in every zone. These parameters are not listed in Table 1

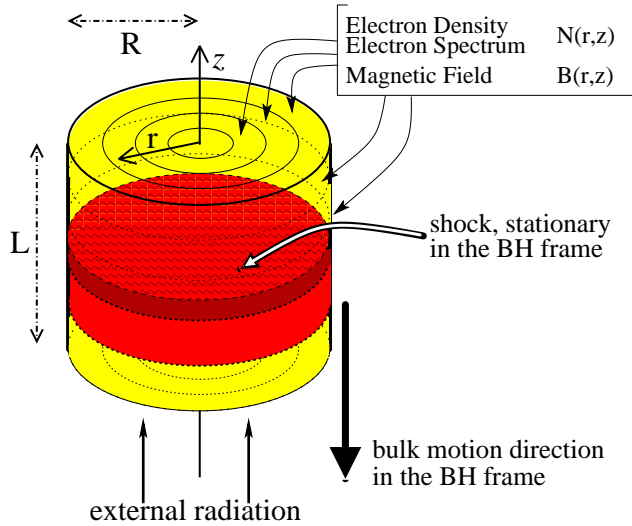


**Figure 1.** The geometry of the model. The volume is divided in the  $r$  and  $z$  directions in zones with their own electron distribution and magnetic field. We also schematically show the setup for the variability of the simulations with a shock. The hatched layer represents a stationary shock. The blob moves downward and crosses the shock front. For illustration purposes, we plot in lighter color shade the zones that crossed the shock at earlier times and have had some time to radiate the newly injected energy. In this representation the photons from the external radiation fields, beamed in the blob rest frame, enter the blob from the bottom surface.

because their relevance is minimal; they are simply seeding each zone with electrons at beginning of the simulation, and they do not represent the electron distribution once the simulations starts. The actual electrons distribution in each zone will be different from the seeded one, and from zone to zone, as they evolve separately. In the steady state it would approximate a power-law like distribution, with  $\gamma_{\min}$  determined by the energy of the picked-up electrons. The spectral index is related to  $t'_{\text{acc}}$  and  $t'_{\text{esc}}$ , with faster escape and slower acceleration generally leading to softer spectrum. The  $\gamma_{\max}$  is determined by the competition between acceleration and cooling, with faster cooling meaning smaller maximum electron energy.

### 3.2 External Radiation

The relativistic jets in Active Galactic Nuclei (AGN) may reside in dense external radiation environments, with contributions from the BLR (Tavecchio & Ghisellini 2008; Poutanen & Stern 2010) or the warm dust of the molecular torus hypothesized to exist beyond the accretion disk (Malmrose et al. 2011). For a thorough discussion we refer the reader to Ghisellini & Tavecchio (2009).

The dominance of different sources of external radiation is connected to the location of the  $\gamma$ -ray emitting region within the jets. The radiation from the BLR can be dominant only when the emission region is located at sub-parsec distance from the central engine of the AGN. Beyond that distance, the infrared radiation from the dust torus is likely to dominate on parsecs scale (Ghisellini & Tavecchio 2009). Poutanen & Stern (2010) argue that the GeV spectral breaks of FSRQs observed by *Fermi*/LAT are a sign of  $\gamma$ -ray absorption inside the BLR. Meanwhile, Marscher et al. (2010) used the correlation between radio knot appearance and  $\gamma$ -ray flares to identify the location of the emission region at several parsecs from the central engine. We will test the viability of both of these two sources of external photons, and see if they can produce the SEDs and light curves observed.

We regard the big blue bump clearly visible in the SED of PKS 1510–089 when in its lower brightness states as unbeamed thermal emission from the accretion disc, and match the data with a luminosity of  $4 \times 10^{45}$  ergs/s and a temperature of  $3 \times 10^4$  K.

This disc emission is used to estimate the energy density experienced in the blob rest frame while its location is within the radius of BLR,  $R_{\text{BLR}}$ , according to the following transformation equation (Ghisellini & Madau 1996):

$$U'_{\text{BLR}} \sim \frac{17}{12} \frac{f_{\text{BLR}} L_{\text{d}} \Gamma^2}{4\pi R_{\text{BLR}}^2 c} \quad (1)$$

where  $L_{\text{d}}$  is the disc luminosity.

Similarly, assuming for simplicity that the region where radiation from the dusty torus yields a significant energy density can be described as a spherical volume of radius  $R_{\text{IR}}$ , the energy density within this region as seen in the blob rest frame can be estimated by

$$U'_{\text{IR}} \sim \frac{f_{\text{IR}} L_{\text{d}} \Gamma^2}{4\pi R_{\text{IR}}^2 c} \quad (2)$$

(Ghisellini & Tavecchio 2009).

For the spectrum of BLR emission, we consider two cases: an approximation as a plain single temperature blackbody peaked at  $1.5\Gamma\nu_{\text{Ly}\alpha}$ , or a more realistic spectrum obtained by taking the unbeamed BLR spectrum in Fig. 4 of Tavecchio & Ghisellini (2008) and beam it according to the equation:

$$U'(\nu') = \frac{2\pi}{\Gamma\beta c} \nu'^2 \int_{\nu_1}^{\nu_2} \frac{I(\nu)}{\nu^3} d\nu, \quad (3)$$

here  $\nu_1 = \nu'/[\Gamma(1 + \beta)]$ ,  $\nu_2 = \nu'/\Gamma$ ,  $I(\nu)$  is the unbeamed intensity spectrum,  $\nu$  and  $\nu'$  are the frequency in the observer's frame and blob frame respectively.

For the infrared emission from the hot dusty torus, we use a blackbody spectrum with temperature (Ghisellini & Tavecchio 2009):

$$T'_{\text{IR}} = 370 \Gamma (1 - \beta \cos \alpha) \text{ K} \sim 370 \Gamma \text{ K}, \quad (4)$$

where  $\alpha$  is the angle between the jet axis and the line connecting the source and the jet, so  $\alpha \sim \pi/2$  for the torus.

For computational ease, we simplify the model by assuming that all the external photons are traveling in the upward direction in the frame of the blob, as illustrated in Fig. 1. All the external photons enter the blob through the lower boundary and the external flux is just the energy density times  $c$ . This is a valid approximation for the typical (large) values of the Lorentz factor appropriate for blazars, which we adopt for ease of computation, although our code allows to setup the flux from the external illuminating source with an angular distribution.

To produce the observed SEDs the disc emission is added as a non-varying component to the beamed emission from the jet in the post-processing of the simulation results.

### 3.3 About model parameters freedom and constraints

In the EC models, we have 5 basic observables (variability time-scale  $\tau_{\text{var}}$ , synchrotron luminosity  $L_{\text{sync}}$ , estimated IC peak frequency  $\nu_{\text{IC,p}}$ , IC luminosity  $L_{\text{IC}}$ , and  $\gamma$ -ray spectral index  $\alpha_{\gamma}$ ) to constrain 6 free parameters ( $R$ ,  $B$ ,  $n_e$ ,  $f_{\text{ext}}$ ,  $\gamma_{\min}$  and  $p_{\text{inj}}$ ). However, there are in fact additional constraints available to further limit the usable range of parameter space. For example, as we will discuss later, in the EC cases the SSC flux can not be too high in order to be consistent with the moderate X-ray variability, which in turn translates into a requirement on the magnetic field strength to be sufficiently large. On the other hand, the required diffuse stochastic acceleration time-scale ( $t'_{\text{acc}}$ ) and hence the cooling time-scale can not be too short, which then imposes a limit on how large the magnetic field can be.

Moreover, as already noted, the value of  $p$  and  $\gamma_{\max}$  in the quiescent state are not direct input parameters. They are the results of the combination of  $t'_{\text{acc}}$  and  $t'_{\text{esc}}$  (and the relevant cooling time-scale). The synchrotron peak frequency  $\nu_{\text{sync,p}}$  is not always used as a constraint because for the physical conditions of our simulations it is not a result of the electron distribution, but it is often determined by synchrotron self-absorption. At the same time, observationally its position in the SED is only poorly constrained by currently available data.

For some other parameters, such as the bulk Lorentz factor of the jet, the radius of the BLR or torus regions, values are set on the basis of empirical estimates obtained by independent studies and therefore may not be regarded as truly free parameters. On the other hand, because the energy density of the external radiation in the blob frame,  $U'_{\text{ext}} \sim f_{\text{ext}} \Gamma^2 / R_{\text{ext}}^2$ , and  $L_{\text{EC}} / L_{\text{sync}} \sim U'_{\text{ext}} / B^2$ , a given SED or set of SEDs will impose a relationship between these parameters.

The size-scales of BLR and torus is generally found to follow a relationship like  $R \sim L_{\text{disc}}^{1/2}$ , with some range in the normalization typically yielding a  $R_{\text{BLR}} = \text{few} \times 10^{17}$  cm and  $R_{\text{IR}} = \text{few} \times 10^{18}$  cm for a disc luminosity of the order of that inferred in PKS 1510–089 on the basis of the observed BBB. We thus decided to set  $R_{\text{ext}}$  to the value closed to the ones expected

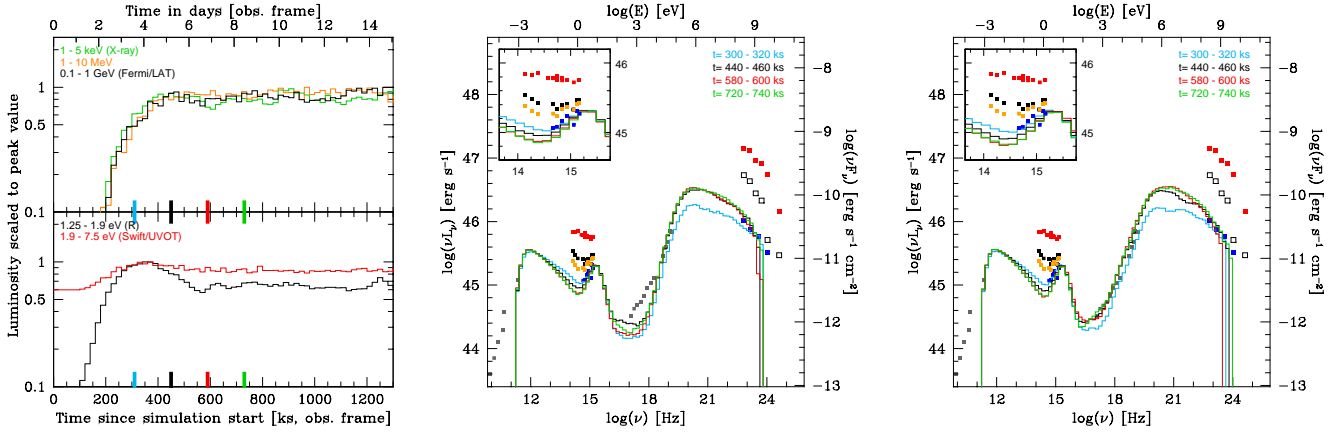


**Figure 2.** **Left, middle:** Light curves and SEDs for the quiescent state of the EC/BLR model, using a blackbody approximation for the BLR spectrum. The histograms in both figures are the results of our simulation, with the energy band chosen shown in the legend of the left figure. The SED snapshots times are shown in legend of figures and marked with matching color segments in the light curves plot. In this and all the paper SED plots the data points are multiwavelength SEDs of PKS 1510–089 mostly in the spring of 2009 from Abdo et al. (2010a) and D’Ammando et al. (2011). The optical/infrared points, also show in the inset, are for the following dates: blue for March 10, orange for March 18, black for March 19, red for March 25/26 (flare peak). The  $\gamma$ -ray, *Fermi*/LAT spectra are: blue squares for the quiescent state of the early 2009 (see Abdo et al. 2010a), red squares the end of March 2009 flare, black empty squares an earlier weaker flare (flare ‘a’ in Abdo et al. 2010a) which we show as a plausible reference for the gamma-ray state before and after the March 2009 flare. The gray points in radio, submm and X-ray are not strictly simultaneous but we regard them as representative because of the very modest variability exhibited by the source during those months in these bands. The X-ray data include the XRT data averaged during the March 2009 flare, and five year integrated BAT data in hard X-rays. **Right:** The SEDs for the quiescent state of the BLR model using the Tavecchio & Ghisellini (2008) BLR spectrum (parameters are listed in Table 1,  $n_f/b_{\text{BLR}}$ ).

from these estimates and given the uncertainty on the  $f_{\text{ext}}$  to regard its value as a free parameter controlling the normalization of the EC emission.

## 4 RESULTS

As illustrated in Section 2 our aim is to reproduce the quiescent and flaring states of PKS 1510–089.

We model a flare as being caused by an injection of relativistic electrons ascribed to the effect of the interaction of the blob with a standing shock, as described in Section 3.1. As the shock travels through the blob (in the blob frame) it injects new particles locally, i.e. in the zones where it currently resides. These newly injected electrons are treated in the same way as all other electrons in each zone; they radiate through synchrotron and IC, and evolve according to the same Fokker-Planck equation.

We will review cases with BLR or torus as the dominant sources of external photons for EC, as well as a pure SSC model, and compare light curves and SEDs with those of the March 2009 observations of PKS 1510–089. In discussing the comparison we will mainly focus on the SEDs, in particular on the infrared, X-ray and  $\gamma$ -ray bands. The light curves, which we show for several observable bands, provided an important constraint guiding the analysis and identifying suitable parameter values but they do not illustrate the differences between different cases as clearly as the comparison of data and SEDs for multiple epochs. This is also due to the fact that purely in terms of intensity variation in narrow bands, the longest time-scale dominates (modulates) the time profile of a flare, and in the cases discussed here the source crossing time is larger than time-scales for electron processes. This was not true for instance for Mrk 421, for which as shown in Chen et al. (2011b) the light curve profiles for various X-ray and TeV bands were different depending on whether the particle related time-scales were faster or slower than the source crossing time, providing us with additional diagnostics.

### 4.1 Quiescent state: no shock

First we try to reproduce the quiescent state SED using as reference the period of the last three months of 2008 during which the  $\gamma$ -ray flux measured by *Fermi*/LAT remained low and with small variations (the ‘quiescent’ period in the naming adopted in Abdo et al. 2010a). We begin with using the blackbody approximation for the spectrum of the BLR emission. We show the results of this simulation in Fig. 2, with the parameters used listed in Table 1.

In this simulation particle injection is exclusively given by the steady-state pick-up term  $Q_{\text{pick}}$ . Because there is no flaring activity, the flux level at every wavelength reaches the steady state after a few light crossing times, and the light curves remain almost flat except for statistical fluctuations.

It is interesting to note that the R-band light curve reaches a flux level higher than the quiescent level before it reaches steady state (effect noticeable also in the SED in the infrared band). This is because the external photons need some time (of the order of one light crossing time) to diffuse through the whole blob<sup>1</sup>. During that time some zones which have not yet received the external photons will experience significantly less IC cooling (which is dominant over synchrotron cooling in this case). Hence the higher energy portion of their electron spectrum will remain at a relatively higher level and produce a relatively more intense synchrotron radiation during this phase. This is an example of how the light travel time effect can affect the actual physics in the jet, not only just the way we perceive the emission. While in this particular case the initial phase of the simulation and particle evolution is not of astrophysical interest, this effect is realistic and illustrates one important

<sup>1</sup> The same is true for the internally produced synchrotron photons scattered by SSC. Their contribution to the photon field in each location will need a time of the order of the light crossing time to stabilize, or, in the case of variable synchrotron emission, to respond to the changes of intensity happening elsewhere in the blob.

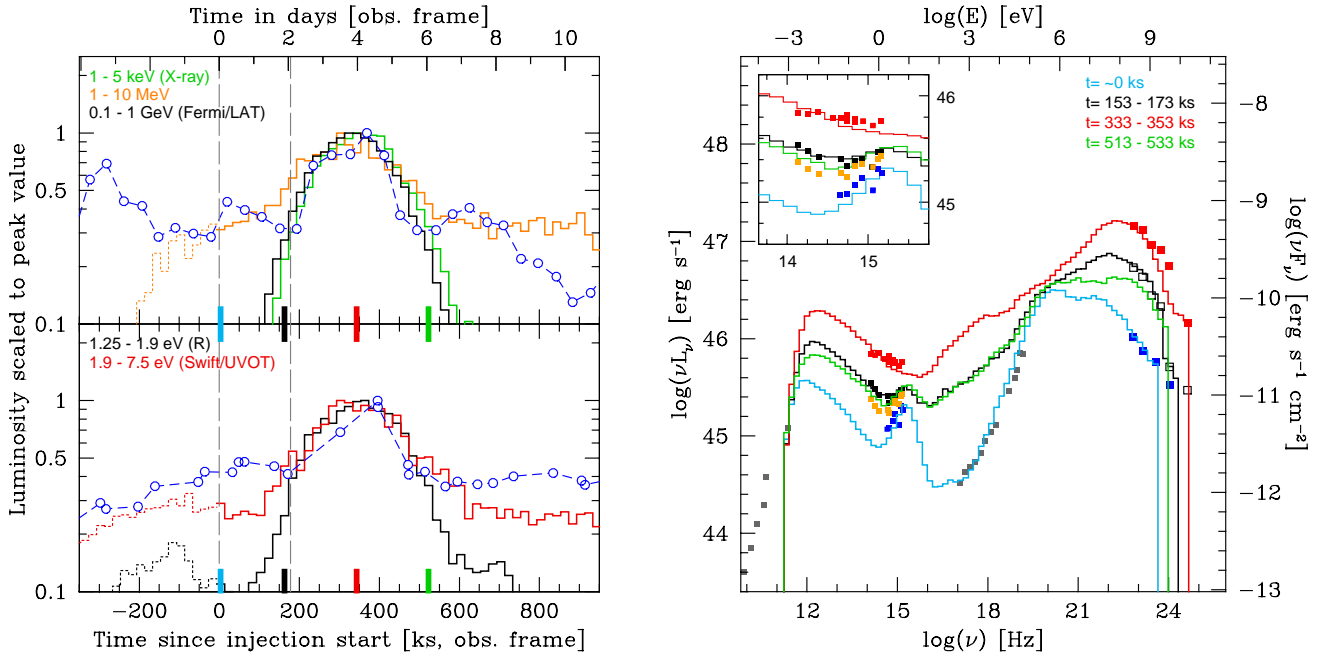


**Figure 3.** Light curves (left) and SEDs (right) for the first EC/BLR scenario. In these and all following light curve plots the blue circles in the lower panel show the observed R-band light curve in March 2009 from the GLAST-AGILE Support Program (GASP), those in the upper panel show the *Fermi*/LAT light curve above 0.2 GeV in March 2009, simultaneous with the R-band data (Abdo et al. 2010a). The SED data points are the same as those in Fig. 2. Simulation light curves are dotted before  $T = 0$  to emphasize that that interval should be regarded as a setup time for the simulated region. The two grey vertical dashed lines mark the start and end of the injection time, i.e. the time during which the shock is crossing the blob. The SEDs correspond to the times (in the observer frame) given in the legend, and marked with colored ticks in the light curves plot. Model parameters are given in Table 1,  $b_{1r15}$ .

aspect of taking into account the finite size of the source and the effect of light travel time on the physical evolution of the system and its emission.

The SEDs match the low state data points at optical and  $\gamma$ -ray frequencies pretty well. The radio data points do not match because it is likely that the radio emission comes from additional emission regions rather than just the one producing the optical and  $\gamma$ -ray emission. The simulated spectrum in the X-ray regime is much harder than the observed one. This improves significantly by using a more detailed description of the BLR spectrum such as that discussed by Tavecchio & Ghisellini (2008), as shown by the SEDs in Fig. 2, where we used a BLR spectrum obtained from their analysis. This confirms their conclusion that an accurate treatment of the BLR spectrum used for the EC emission is necessary in producing the spectrum in the soft to medium X-ray band ( $\sim 0.1$ – $10$  keV), where usually high quality data are available. This band is of critical importance because it can provide constraints on the relative contribution of SSC and EC, and also on the characteristics of the lower energy end of the electron distribution.

#### 4.2 EC/BLR: shock crossing with $\Gamma = 15$

Starting from a baseline quiescent state like the one just discussed, we model the flare for a case in which the dominant EC contribution is from the BLR. For this first case we adopt a blob bulk Lorentz factor  $\Gamma = 15$ . The results are shown in Fig. 3. Light curves show that the optical/infrared variability is larger in the R-band than in the bluer *Swift*/UVOT bands, due to the contribution of the non-variable big blue bump emission in the UV. This is consistent with observations.

Both the X-ray light curve and the SEDs clearly show that our

simulations predict large-amplitude variations in the X-ray flux. This is at odds with observations which show only modest X-ray variability (less than a factor of 2) throughout the entire 2009 observing campaigns, including the largest flares. The excessive X-ray variation in our simulations is the result of SSC emission. Although currently our model does not track separately photons of EC and SSC origin, the parameters we use indicate that emission by SSC is not negligible in the X-ray band even in the quiescent state. In case of a flare caused by changes in the electron spectrum and/or density the amplitude of variation of the SSC emission will always be larger than that of the synchrotron (as long as we are considering electrons scattering in the Thomson regime, which is the case here). Therefore as we model the factor of 10 increase of the non-thermal emission in the optical/infrared band the corresponding IC emission will vary by a factor up to a 100, with a large contribution in the X-ray band.

This SSC variation makes this model and parameter set not consistent with the observed features of PKS 1510–089. This example also illustrates the importance of modeling the time evolution of the SED, rather than simply modeling with sets of parameters left fully free to vary between different epochs the high and low state SEDs, or even sequences of SEDs taken close enough in time during a single flare that they are very likely to be related to each other as part of the development of a single event.

##### 4.2.1 Quiescent vs. flaring state and the importance of time-dependent multi-zone modeling

The comparison between the SEDs of the steady and flaring states shown in Figures 2 and 3 illustrates another important difference between a time-dependent multi-zone simulation and a one-zone



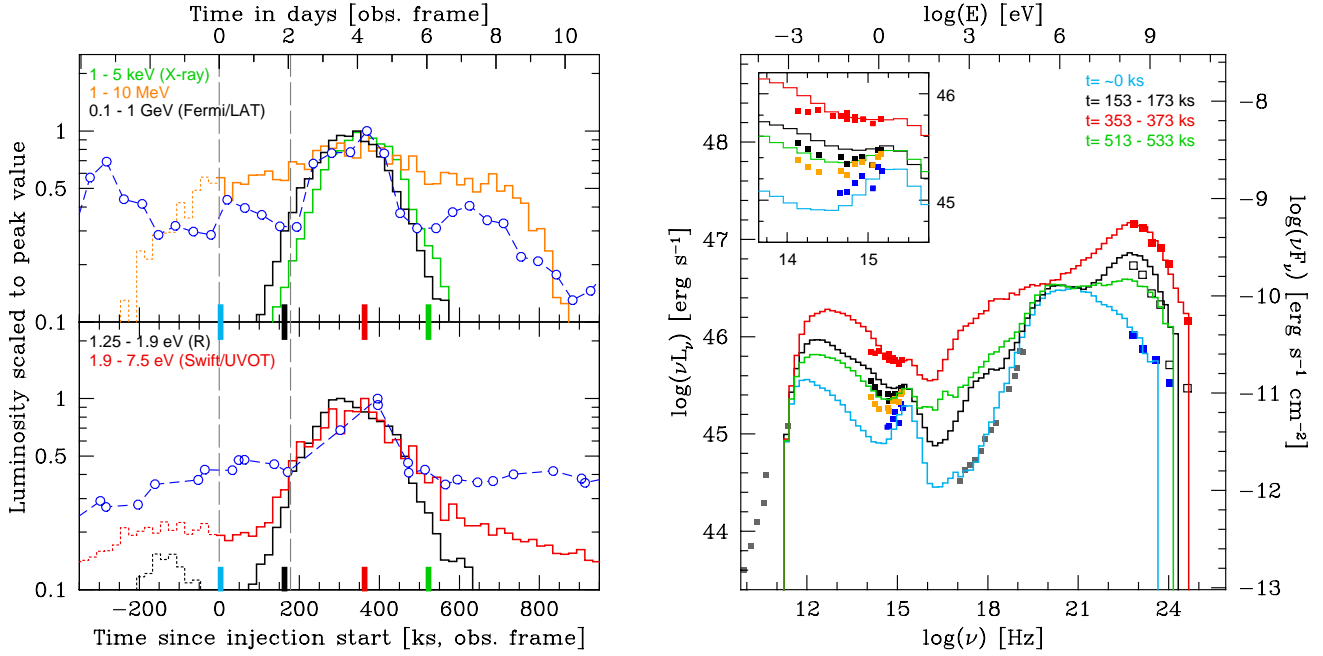


**Figure 4.** Same of Figure 3 for the second case of EC/BLR flare simulations, with  $\Gamma = 15$  and higher minimum energy for the injected electrons,  $\gamma_{\min} = 90$  (see Table 1, `blr15highmin`).

(effectively point-like) simulation, for which the quiescent case can be considered a proxy<sup>2</sup>: the SEDs of the more realistic model are significantly more complex in the shape and variation of the high energy component. This is the result of both internal and external LTTE giving to the observer a mix of emission produced at different times in zones at different stages of the flare development and with electron distributions at different stages of their evolution.

Even if locally the processes affecting the electrons are fast and the particle spectrum could be regarded as reaching rapidly a steady state (in case of injection lasting for a long enough time), the sequence of steady state SEDs produced in a flare is not equivalent to a sequence of steady state SEDs (see Bonnoli et al. 2010, for an example of this approach applied to the FSRQ 3C 454.3).

Admittedly in this paper we are presenting one possible scenario for the flaring state of a FSRQ, but this type of differences can be expected to exist for a wide range of plausible scenarios of variable emission from a relativistic jet.

### 4.3 EC/BLR: $\Gamma = 15$ , with higher $\gamma_{\min}$

A potential remedy for the excessive X-ray variability crisis could be to increase the minimum energy of the injected electrons. The peak of the emission of the variable component, driven by the electron injection, is determined by the electron's  $\gamma_{\min}$ . A higher  $\gamma_{\min}$  may push the SSC emission by these electrons to peak at a higher frequency where it can be ‘hidden’ beneath the rapidly rising stronger EC emission. However,  $\gamma_{\min}$  is fairly constrained by the observed MeV-GeV  $\gamma$ -ray spectrum, namely by the fact that we do not observe a spectral turn over in the *Fermi*/LAT data. Too large a  $\gamma_{\min}$  will produce a EC SED peaking in the *Fermi*/LAT observa-

tional band. With this in mind, we tested one case with a slightly higher injected  $\gamma_{\min} = 90$ . The results are shown in Fig. 4.

The peak of the EC SED in this case is shifted close to the lowest energy data point of the *Fermi*/LAT spectrum, indicating that  $\gamma_{\min} = 90$  is already of the order of the largest value that we can use with the current BLR spectrum and a Lorentz factor of 15. On the other hand, while there is some change on the spectral shape of the high state X-ray spectra, the fundamental problem of the excessive amplitude of its variation is not mitigated. The inconsistency between the observed and simulated X-ray variability remains a problem in the higher injected  $\gamma_{\min}$  case.

### 4.4 EC/BLR: higher Lorentz Factor, $\Gamma = 25$

Instead of moving the SSC emission in frequency, another route to solve the X-ray variability inconsistency may be to decrease the level of the SSC emission relative to the other components. In order to do this while keeping the same level of synchrotron emission, we need to decrease the ratio between the synchrotron (SSC seed photons) energy density and the magnetic energy density. We can achieve this by increasing the Doppler factor because in that case the synchrotron energy density in the blob frame needs to decrease accordingly to match the optical data. This requires to change the values of other parameters to produce a SED well fitting the observed one. The modified parameters are reported in Table 1. The results are shown in Fig. 5.

In this case, the luminosity in the X-ray dip between the two main components is indeed lower. Nevertheless because any SSC emission occurring in this band would still be varying by a factor larger than that of the optical flux, the range of the X-ray variation remains large, and easily exceeding the constraint set by the well measured X-ray intensity and spectrum. However, since in this case the quiescent X-ray flux is lower than the observed one, it may be possible to explain the X-ray band spectrum as comprising a contribution from additional, relatively cooled blobs, which would

<sup>2</sup> The steady state emission is effectively equivalent to what would be produced by a one-zone non-time-dependent code.

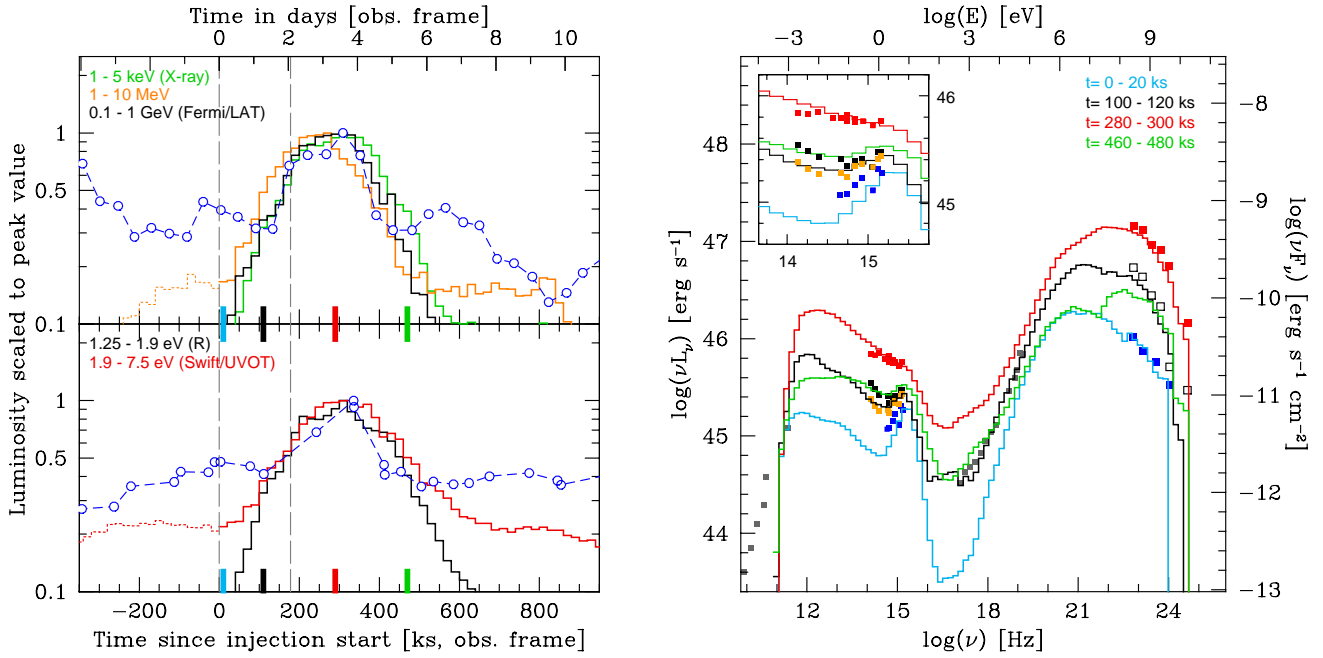


**Figure 5.** Light curves (left) and SEDs (right) for the EC/BLR case with higher bulk Lorentz factor,  $\Gamma = 25$ . Parameters are given in Table 1, b1r25.

partially dilute the large variation. However, even taking that into account, considering the spectral variability present in the varying X-ray component, it may not be straightforward to reconcile the overall X-ray properties with the remarkably stable observed spectra.

#### 4.5 EC dominated by IR emission from the torus

Emission from hot dusty, molecular, gas in the putative torus surrounding the accretion disk is another plausible source of external photons in the immediate environment of the relativistic jet. This scenario is motivated by the observation of the coincidence of  $\gamma$ -ray flares with the appearance of new knots in radio images of PKS 1510–089 (Marscher et al. 2010). These observations hint that the emission region responsible for  $\gamma$ -ray flares is located at parsec scales, which is beyond the usually inferred radius of the BLR (Kaspi et al. 2007; Bentz et al. 2006, 2009). At this distance, the IR torus (Pier & Krolik 1992b,a) becomes the main candidate as the source of EC seed photons (Ghisellini & Tavecchio 2009; Sikora et al. 2009).

We calculate the energy density and temperature of the torus emission according to equations (2) and (4). Because the energy density and SEDs of the emission from the torus are very different from those of the BLR, it is necessary to change the values of several parameters to be able to match the quiescent and then flaring states. The best set of parameters is reported in Table 1, and the light curves and SEDs in Fig. 6.

The broadband SEDs compare reasonably well with observations; the light curves vary on a time-scale consistent with the data; the optical and  $\gamma$ -ray light curves are well correlated with no significant lags; the variations in the optical and  $\gamma$ -ray bands have similar amplitude; the variations in the UV band are less prominent than those in the optical. However, it is worth noting that it has proven to be difficult to concurrently match the GeV spectrum and the soft slope through the infrared bands. Although we can not claim to have achieved a perfect match in the latter in the previous cases, this is an issue that did not seem to emerge as seriously as here.

The problem of X-ray variability in this case is similar to the one in the BLR case. It is likely that similarly to the previous case, a higher Doppler factor would lower the flux produced by SSC in the X-ray band.

One of the main differences between the torus emission and the BLR emission as source of EC seed photons is that the owing to its lower temperature the torus radiates at lower frequency compared to the BLR. This means that to scatter these seed photons to the same  $\gamma$ -ray energies, the energy of the electrons needs to be higher than those needed in a BLR scenario. In the context of the scenario presented in this work, this means that more efficient particle acceleration is needed to sustain the high energy electrons, which have faster cooling times. This also means that faster particle escape is to be expected in the torus scenario, otherwise the accelerated particles will not form a power-law distribution that can produce emission with the observed spectral shape. It turns out that the value for the particle escape time-scale parameter needed in this case may be too fast to be realistic ( $t'_{\text{esc}} = 0.015 Z/c$ ). However, it is worth emphasizing that, chosen name notwithstanding, the ‘escape’ term in the kinetic equation may be regarded as a crude approximation for a describing a generic energy independent process affecting electrons, and in this sense a value significantly smaller than the source crossing time may not be automatically be considered unphysical. Nevertheless, because the time-scale for plausible candidate such as actual escape or adiabatic cooling processes would likely be of the order of  $Z/c$ , it would certainly be desirable to not be forced to such extreme values for  $t'_{\text{esc}}$ , and we regard this as a serious problem for EC on torus emission, in the framework discussed here.

#### 4.6 Pure SSC

We already cited some of the recent results suggesting that the active,  $\gamma$ -ray emitting region, in the jets of several blazars may be located beyond the size-scale of the BLR on the basis of correlated multiwavelength variability and VLBA imag-



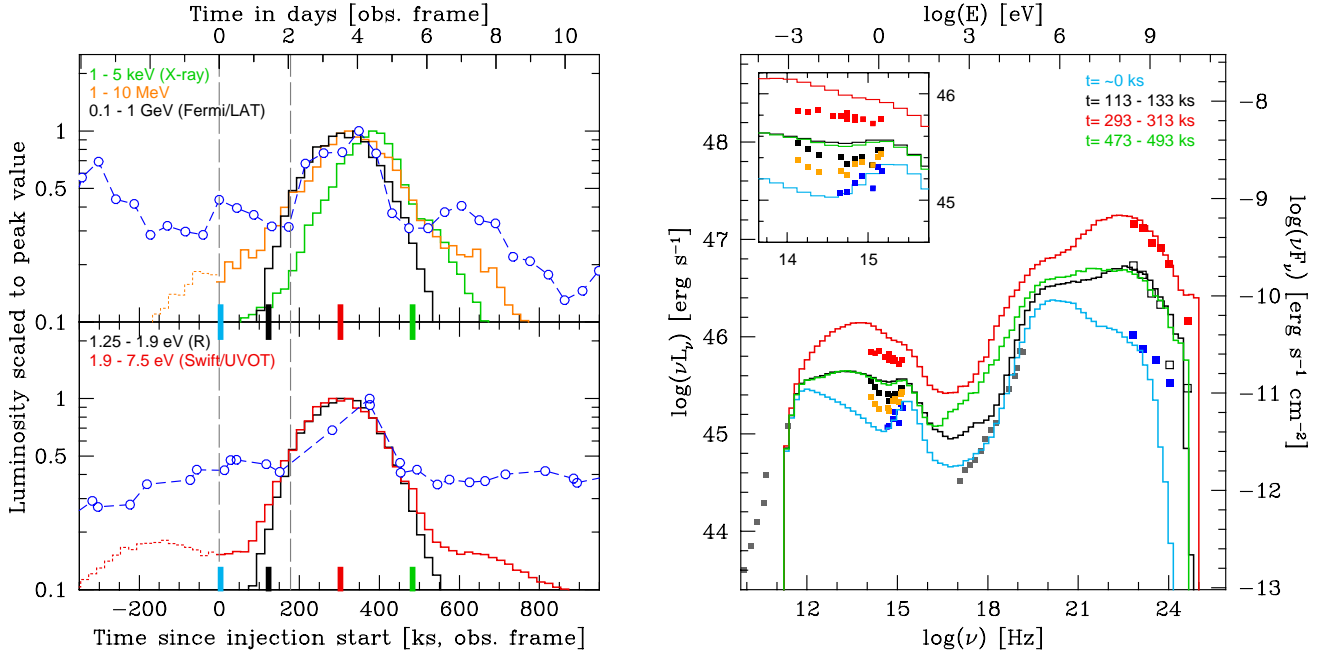


**Figure 6.** Light curves (left) and SEDs (right) for the case with the EC dominated by radiation from the torus. Parameters are listed in Table 1,  $\tau_{\text{torus15}}$ .

ing (Larionov et al. 2008; Sikora et al. 2008; Marscher et al. 2010; Agudo et al. 2011a,b). Additionally, the detection in TeV  $\gamma$ -rays of a few FSRQs, including a recent confirmation for PKS 1510–089 (Cortina et al. 2012) (others are 3C 279, Albert et al. 2008; Aleksić et al. 2011a, and PKS 1222+216, Aleksić et al. 2011b), challenges traditional EC scenarios because jet emitted TeV photons would be readily lost by photon-photon pair production with the copious soft photons surrounding the jet. These findings have thus stimulated a renewed interest in the possibility that even for some of these powerful jets in systems with luminous accretion disk and broad line emission, the  $\gamma$ -ray emission may be predominantly by SSC (for analysis on 3C 279 see e.g., Böttcher et al. 2009). Finally, studying a large sample of well characterized blazars detected by *Fermi*/LAT and with an estimate of their jet intrinsic power, Meyer et al. (2012) find that, while for the highest jet power objects there is a clear collective sign of EC being the dominant mechanism for their  $\gamma$ -ray emission, the properties of the rest of the population are consistent with SSC.

Moreover, as discussed in the previous sections, our simulations of EC models for the type of flaring blob scenario presented here show large variability in X-ray which is inconsistent with the very robust observational finding of lack of significant variations even during the flaring phase, and which is caused by the SSC contribution. The existence of this latter is unavoidable, and our tests suggest that even mitigating its effect is not a trivial endeavor (§ 4.3, § 4.4).

Therefore, it seems natural to want to test if we could reproduce the benchmark observations with a pure SSC scenario. The results are shown in Fig. 7.

The SSC model reproduces well several aspects of the observations. In particular, the amplitude of the flux variability and the spectral change in the X-ray band are overall much closer to what was observed. The *Fermi*/LAT band spectrum and intensity is also well matched. Because of the presence of the steady disk emission mostly contributing to the blue/UV flux, the flux in the R-band varies less than the *Swift*/UVOT band.

However, the simulations produce an X-ray spectrum consistently harder than the one observed, mostly determined by the sharp ‘cut-off’ of the lower energy end of the electron distribution. The observed SED, namely the very hard X-ray spectrum, constrains this latter to a fairly high  $\gamma_{\text{min}}$ , much larger than the values used in the EC cases. The simulated infrared spectrum is also somewhat harder than the spectrum observed in the intermediate state. Finally, the frequency at which the synchrotron spectrum peaks tends to be too high, which is a consequence of the high  $\gamma_{\text{min}}$  required by the X-ray spectrum. Since the SSC model has fewer free parameters than the EC model, they are more constrained than those in the EC models, and do not leave us much freedom for improving significantly on these issues.

## 5 DISCUSSION AND CONCLUSIONS

We have modeled multiwavelength variability produced in the jet of PKS 1510–089, with EC model involving external radiation from BLR or dusty molecular torus, as well as pure SSC model.

As discussed also by Tavecchio & Ghisellini (2008), the use of a realistic BLR spectrum seems indeed to be critical to model accurately the inverse Compton component, in particular its lower energy end which is observed in great detail in the X-ray band, thus providing a powerful diagnostic on model parameters. The results presented here, namely the challenging issue of the large X-ray variability caused by the SSC contribution, which has a distinctly different spectral shape from the EC, further strengthen the importance of modeling as accurately as possible the source of the EC seed photons.

In the same context, we should comment on the fact, noted in Section 3.3, that in order to obtain reasonable SEDs and light curves in the EC/BLR cases we had to adopt a reprocessed fraction of BLR luminosity,  $f_{\text{BLR}}$ , that is significantly smaller than what one would expect. A more traditional  $f_{\text{BLR}}$ , such as 0.1 in Ghisellini & Tavecchio (2009), would yield a more intense BLR

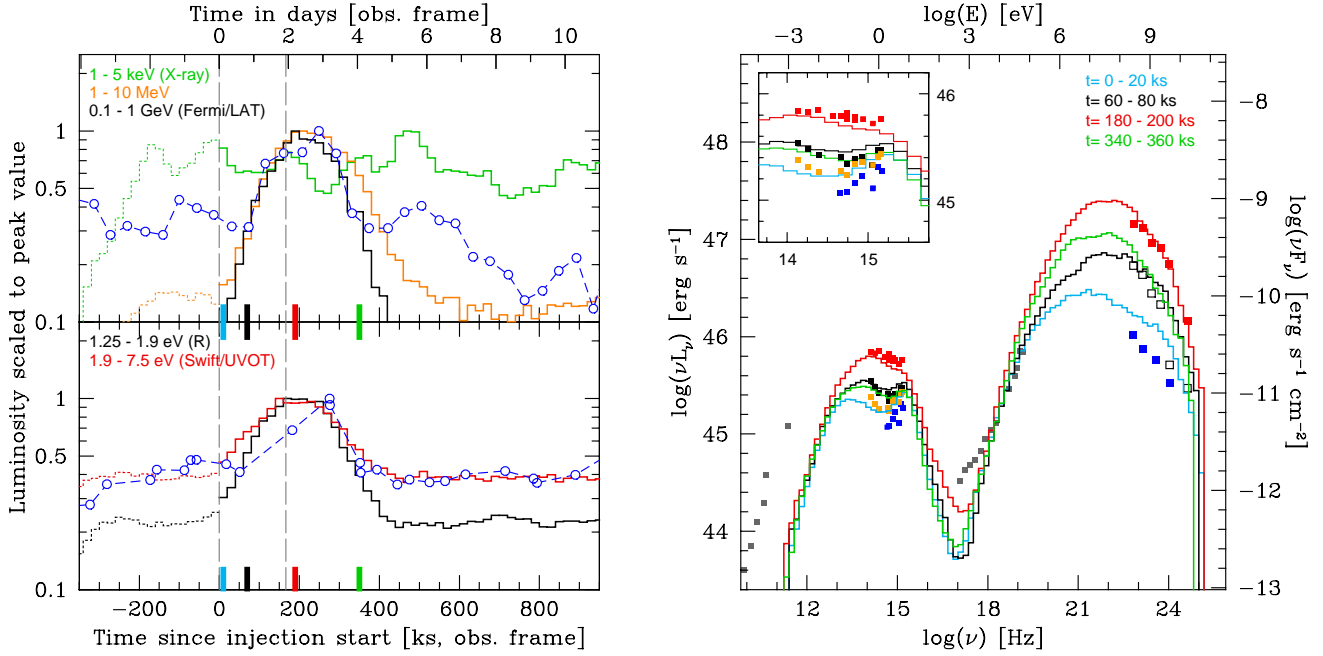


**Figure 7.** Light curves (left) and SEDs (right) for the SSC case. Parameters are listed in Table 1, *ssc*.

radiation energy density and the increased electron energy loss rate in the blob would push the model towards fairly extreme values for several of the parameters. This could be regarded as an indication that the general scenario that we studied in this work may not be a suitable explanation for flares in FSRQs. On the other hand, this scenario yields acceptable, though not perfect, results for the EC/torus and the SSC cases.

As discussed in Section 3.3, the combination of  $(f_{\text{ext}} \Gamma^2 / R_{\text{ext}}^2) / B^2$  is related to the ratio between the IC and the synchrotron luminosities (Compton dominance), which is an observable. Although its value may vary during a flare, the value of the Compton dominance imposes a relationship between those parameters of the source (hence model). A given source or source state may have a preferred value for the Compton dominance which should be matched by a combination of  $f_{\text{ext}}$ ,  $\Gamma$  and  $R_{\text{ext}}$  (and  $B$ ), independently on whether one wants to model it with EC/BLR or EC/torus. For the Compton dominance ratio that seems to work well for PKS 1510–089 it is possible to adopt plausible values of  $R_{\text{ext}}$  and  $f_{\text{ext}}$  for the EC/torus case and less so for the EC/BLR case. This consideration does not depend strongly on the scenario adopted for the the blob and the mechanism causing outbursts and it may suggest that indeed PKS 1510–089 may not be modeled by EC/BLR in general. Alternatively, it could mean that our naive idea of the BLR and torus does not represent their real structure and causes the EC/BLR model to fail to match the data. Another possibility is that, the relativistic jet in this source has a milder bulk Lorentz factor  $\Gamma$  than 15 or 25 that we adopted in this paper. However this is in conflict with the high  $\Gamma$  required to avoid the large SSC contribution.

Leaving aside the above considerations, and looking at the results of the simulations as run with the best fitting parameter sets, it is difficult to identify a clear superiority for any of them. None can be convincingly excluded.

The EC/BLR scenario suffers the problem of the large X-ray variability, and it produces better, marginally satisfactory, results if we adopt a larger value for the bulk Lorentz factor, which is still

within the observed range. It also requires parameters for the BLR which are at least unusual.

The EC/torus also has the problem of highly variable SSC in the X-ray band, which we can expect to be mitigated by using a larger Lorentz factor, and it works with reasonable parameters for the external radiation component, but it requires very fast particle acceleration and escape time-scales to maintain the balance between acceleration and cooling for the high energy electrons necessary to scatter to the GeV band the lower energy external photons.

The pure SSC model naturally addresses the X-ray variability issue, but at price of very high minimum electron energy to avoid significant emission in X-rays, which in turn make it difficult to reproduce the synchrotron peak region SED and makes the X-ray spectrum significantly harder than the observed one. Because its GeV emission comes from scattering lower energy photons than the EC/BLR case, like the EC/torus case the SSC requires fast escape time-scale, though less extreme, which could be considered a serious problem.

In all three cases, their X-ray problems may be relaxed if there is a slowly varying contribution from other emission regions, filling the dip between the synchrotron and IC components, softening the X-ray spectrum and diluting its variations.

Overall, while within the framework studied in this work we can not firmly discriminate the three main scenarios, and the framework that we adopted is just one possibility, our results show clearly the differences produced by a more realistic treatment of the emitting source in the shape of SEDs and their time variability over relevant, observable time-scales.

These results demonstrate that proper modeling of the high quality data produced by the plethora of best multiwavelength campaigns on the brightest *Fermi*/LAT blazars to exploit the wealth of information that they carry and advance our understanding of their physics can only be achieved with time-dependent multi-zone simulations.

Looking forward, there are several aspects of the predicted source variability that we have not discussed, such as more de-

tailed analysis of correlated variability (e.g. time lags). Moreover as shown here, SEDs exhibit complex features and variations and it may be possible to explain the interesting, challenging, observation of large break in the *Fermi*/LAT spectra seen in a handful of sources, comprising both FSRQs and low-peaked BL Lacs (Abdo et al. 2010c). The observed breaks are larger than what would be produced by cooling and too sharp to be consistent with an exponential cutoff. Several ideas have been proposed to explaining them as due to external factors, namely  $\gamma\gamma$  absorption outside the jet (Poutanen & Stern 2010; Finke & Dermer 2010; Ackermann et al. 2010), and some are somewhat inconsistent with other multiwavelength properties.

Finally, in these simulations we have used a simple model of energy independent particle acceleration, whereby in order to maintain a power-law electron distribution with a certain slope, the particle escape time-scale is tied to the acceleration time-scale. The fast radiative cooling in our model requires fast particle acceleration and hence fast particle escape. This required escape time-scale has turned out to be smaller than the limit of  $Z/c$ , which happens if all particles travel freely at the speed of light. However, the actual particle acceleration process is expected to have a more complicated energy dependence than assumed here. Therefore, the acceleration and escape time-scales derived here are only for instructive purposes. We will investigate whether a more realistic energy dependence of the particle acceleration process may change the required acceleration and escape time-scales.

## ACKNOWLEDGMENTS

We would like to thank Fabrizio Tavecchio and Gabriele Ghisellini for providing their BLR spectra. This research has been supported by NASA grants NAG5-11796, NAG5-11853, NNX12AE43G, *Chandra* GO AR9-0016X, and *Fermi* GI NNX10AO42G. MB acknowledges support by NASA through *Fermi* GI NNX10AU11G and ATP grant NNX10AC79G. This work was supported in part by the Shared University Grid at Rice funded by NSF under Grant EIA-0216467, and a partnership between Rice University, Sun Microsystems, and Sigma Solutions, Inc. This work was supported in part by the Data Analysis and Visualization Cyberinfrastructure funded by NSF under grant OCI-0959097. This work was supported in part by the Cyberinfrastructure for Computational Research funded by NSF under Grant CNS-0821727. This research has made use of NASA's Astrophysics Data System and of the NASA/IPAC Extragalactic Database (NED) which is operated by the Jet Propulsion Laboratory, California Institute of Technology, under contract with the National Aeronautics and Space Administration.

## REFERENCES

Abdo, A. A. et al. 2010a, *ApJ*, 721, 1425  
 —. 2010b, *ApJ*, 716, 835  
 —. 2009, *ApJ*, 699, 817  
 —. 2010c, *ApJ*, 710, 1271  
 Abramowski, A. et al. 2012, *A&A*, 539, A149  
 Ackermann, M. et al. 2010, *ApJ*, 721, 1383  
 Agudo, I. et al. 2011a, *ApJ*, 726, L13  
 —. 2011b, *ApJ*, 735, L10  
 Aharonian, F. et al. 2007, *ApJ*, 664, L71  
 Albert, J., et al. 2008, *Science*, 320, 1752  
 Aleksić, J. et al. 2011a, *A&A*, 530, A4  
 —. 2011b, *ApJ*, 730, L8  
 Arbeiter, C., Pohl, M., & Schlickeiser, R. 2005, *ApJ*, 627, 62

Bentz, M. C., Peterson, B. M., Netzer, H., Pogge, R. W., & Vestergaard, M. 2009, *ApJ*, 697, 160  
 Bentz, M. C., Peterson, B. M., Pogge, R. W., Vestergaard, M., & Onken, C. A. 2006, *ApJ*, 644, 133  
 Bonnoli, G., Ghisellini, G., Foschini, L., Tavecchio, F., & Ghirlanda, G. 2010, *MNRAS*, 1476  
 Böttcher, M. 2007, *Ap&SS*, 309, 95  
 Böttcher, M., Reimer, A., & Marscher, A. P. 2009, *ApJ*, 703, 1168  
 Chen, X. 2012, PhD thesis, Rice University  
 Chen, X., Fossati, G., & Böttcher, M. 2012, *MNRAS*, in preparation  
 Chen, X., Fossati, G., Liang, E., & Böttcher, M. 2011a, *Journal of Astrophysics and Astronomy*, 32, 185  
 Chen, X., Fossati, G., Liang, E. P., & Böttcher, M. 2011b, *MNRAS*, 416, 2368  
 Chiaberge, M., & Ghisellini, G. 1999, *MNRAS*, 306, 551  
 Cortina, J., et al. 2012, *The Astronomer's Telegram*, 3965, 1  
 D'Ammando, F. et al. 2011, *A&A*, 529, A145  
 Dermer, C., & Lott, B. 2011, *ArXiv e-prints*, 1110.3739  
 Dermer, C. D., Schlickeiser, R., & Mastichiadis, A. 1992, *A&A*, 256, L27  
 Finke, J. D., & Dermer, C. D. 2010, *ApJ*, 714, L303  
 Fossati, G. et al. 2008, *ApJ*, 677, 906  
 Ghisellini, G., & Madau, P. 1996, *MNRAS*, 280, 67  
 Ghisellini, G., & Tavecchio, F. 2009, *MNRAS*, 397, 985  
 Graff, P. B., Georganopoulos, M., Perlman, E. S., & Kazanas, D. 2008, *ApJ*, 689, 68  
 Hinton, J. A., & Hofmann, W. 2009, *ARA&A*, 47, 523  
 Jorstad, S. G. et al. 2005, *AJ*, 130, 1418  
 Kaspi, S., Brandt, W. N., Maoz, D., Netzer, H., Schneider, D. P., & Shemmer, O. 2007, *ApJ*, 659, 997  
 Kataoka, J. et al. 2008, *ApJ*, 672, 787  
 Kataoka, J., Takahashi, T., Makino, F., Inoue, S., Madejski, G. M., Tashiro, M., Urry, C. M., & Kubo, H. 2000, *ApJ*, 528, 243  
 Katarzyński, K., Ghisellini, G., Mastichiadis, A., Tavecchio, F., & Maraschi, L. 2006, *A&A*, 453, 47  
 Katarzyński, K., Lenain, J., Zech, A., Boisson, C., & Sol, H. 2008, *MNRAS*, 390, 371  
 Larionov, V. M. et al. 2008, *A&A*, 492, 389  
 Levinson, A. 2006, *International Journal of Modern Physics A*, 21, 6015  
 Malmrose, M. P., Marscher, A. P., Jorstad, S. G., Nikutta, R., & Elitzur, M. 2011, *ApJ*, 732, 116  
 Mannheim, K. 1998, *Science*, 279, 684  
 Marscher, A. et al. 2010, *ApJ*, 710, L126  
 Meyer, E. T., Fossati, G., Georganopoulos, M., & Lister, M. L. 2012, *ApJ Letters*, in press, TBD, [arXiv:1203.4991](https://arxiv.org/abs/1203.4991)  
 Pier, E. A., & Krolik, J. H. 1992a, *ApJ*, 401, 99  
 —. 1992b, *ApJ*, 399, L23  
 Poutanen, J., & Stern, B. 2010, *ApJ*, 717, L118  
 Pucella, G. et al. 2008, *A&A*, 491, L21  
 Rachen, J. P. 2000, in *Proc. of GeV-TeV Gamma Ray Astrophysics Workshop: Towards a Major Atmospheric Cherenkov Detector VI, Snowbird*, eds. B.L. Dingus, M.H. Salamon, D.B. Kieda, AIP Conf. Proc. 515 (New York: AIP), 41  
 Sikora, M., Begelman, M. C., & Rees, M. J. 1994, *ApJ*, 421, 153  
 Sikora, M., & Madejski, G. 2001, in *American Institute of Physics Conference Series*, Vol. 558, *High Energy gamma-ray Astronomy: International Symposium*, ed. F. A. Aharonian & H. J. Völk, 275  
 Sikora, M., Moderski, R., & Madejski, G. M. 2008, *ApJ*, 675, 71  
 Sikora, M., Stawarz, L., Moderski, R., Nalewajko, K., & Madejski, G. M. 2009, *ApJ*, 704, 38  
 Sokolov, A., & Marscher, A. P. 2005, *ApJ*, 629, 52  
 Sokolov, A., Marscher, A. P., & McHardy, I. M. 2004, *ApJ*, 613, 725  
 Tavecchio, F., & Ghisellini, G. 2008, *MNRAS*, 386, 945  
 Thompson, D. J., Djorgovski, S., & de Carvalho, R. 1990, *PASP*, 102, 1235  
 Tramacere, A., Massaro, E., & Taylor, A. M. 2011, *ApJ*, 739, 66